

Modality-Fair Preference Optimization for Trustworthy MLLM Alignment

Songtao Jiang^{*1}, Yan Zhang^{*2}, Ruizhe Chen¹, Yeying Jin² and Zuozhu Liu^{†1}

¹Zhejiang University

²National University of Singapore

Abstract

Direct Preference Optimization (DPO) is effective for aligning large language models (LLMs), but when applied to multimodal models (MLLMs), it often favors text over image information, leading to unreliable outputs and visual hallucinations. To address this, we propose Modality-Fair Preference Optimization (MFPO) to balance text and image preferences. First, we found that the lack of image-related rewards in preference data biases optimization toward text, so we created automated, fine-grained image preference data to correct this. Then, we designed a learning objective to ensure the model captures both text and image preferences while maintaining high-quality outputs. Finally, we use a multi-stage alignment approach to stabilize training and improve learning across both modalities. Extensive experiments demonstrate that MFPO significantly enhances MLLM trustworthiness. On models like LLaVA-v1.5 (7B, 13B), our approach reduces hallucinations substantially. On the 7B model, MFPO outperforms GPT-4V and achieves a nearly 40% improvement over previous methods on Object HalBench, as well as achieving state-of-the-art performance on both Object HalBench and AMBER when combined with the latest LLaVA-v1.6. Code will be released.

1 Introduction

Direct Preference Optimization (DPO) has proven to be an effective strategy for aligning large language models (LLMs) (Rafailov et al., 2024; Naveed et al., 2023; Kaddour et al., 2023; Zhao et al., 2023a; Liu et al., 2023), and its success extends to multimodal large language models (MLLMs). A key advantage of DPO is its ability to

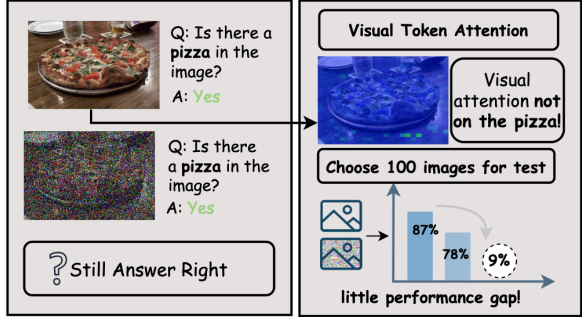


Figure 1: We assess hallucination behavior in LLaVA-v1.5 after preference optimization. Despite severe degradation through diffusion noise (Leng et al., 2024), accuracy dropped by only 9%, suggesting minimal attention to image content during VQA.

enhance trustworthiness by addressing visual hallucinations (Yu et al., 2024a,b; Zhang et al., 2024; Bai et al., 2024; Zhou et al., 2024; Amirloo et al., 2024). Visual hallucinations, where models generate text that inaccurately describes visual content or refers to nonexistent objects, present a critical challenge, particularly in tasks like Visual Question Answering (VQA), where responses must be based on actual visual input (Favero et al., 2024; Huang et al., 2024b; Jing et al., 2020; Ramakrishnan et al., 2018). To address this, preference optimization methods have been applied to reduce hallucinations by training models to prefer accurate responses over hallucinated ones. By treating hallucinated outputs as rejected options, these methods encourage models to learn from accurate responses, thereby enhancing trustworthiness (Wang et al., 2024; Pi et al., 2024; Zhang and Rong, 2024). Current research focuses on creating more refined chosen and rejected preference data through manual annotations and leveraging open-source MLLMs for labeling (Yu et al., 2024a; Sun et al., 2023), while optimization techniques are continuously evolving to align preferences across multiple dimensions (Zhang and Rong, 2024; Zhou et al., 2024; Wang et al., 2024).

^{*} Equal contribution.

[†] Corresponding author.

Work still in progress

While these methods have made some progress in reducing hallucinations, they often neglect the balance between text and image modality preference optimization in multimodal tasks (Wallace et al., 2024; Zhou, 2024). A critical question arises: What has the model learned during preference optimization when rewards are based on text? Is it simply memorizing text preferences, or is it learning to more accurately leverage image information to answer questions? As shown in Figure 1, even with multi-step diffusion noise that compromises the image’s semantic content (Leng et al., 2024), the model still answers the questions correctly. Furthermore, our experiments show that across 100 images, the performance gap between the original images and the semantically degraded ones is only 9%, indicating that the model is not utilizing the image information but rather relying on memorized text preferences. This severely undermines the model’s trustworthiness in answering questions (Shah et al., 2019; Chen et al., 2020; Jiang et al., 2024b; Li et al., 2022; Liang et al., 2020).

To address the issue of balancing preference alignment between modalities and ensuring that text-level optimization incorporates image-based preferences, we propose Modality-Fair Preference Optimization (MFPO). First, we construct image preference data for integrating the image-level reward function. Similar to text preference data, we begin by identifying hallucination-prone regions hinted at in the text. Keywords are extracted using a multipartite graph (Jin and Zhang, 2014; Boudin, 2018), chosen for its ability to model complex relationships between word sets (Dawande et al., 2001). These keywords are mapped to corresponding image regions with the help of a lightweight Segment Anything Model (SAM) (Kirillov et al., 2023). Finally, diffusion noise is applied to generate fine-grained noisy images, serving as rejected preference data. We then develop an image preference reward function that encourages the model to select images with clean regions over noisy ones.

To improve training stability and efficiency, we adopt a curriculum learning-inspired hierarchical preference alignment method (Bengio et al., 2009; Matiisen et al., 2019), categorizing data into easy, medium, and hard levels based on model confidence. This easy-to-hard paradigm allows the model to progressively refine both text and image preferences. Additionally, we incorporate margin loss to maintain reward consistency for preferred responses, ensuring stable training. Our method

balances text and image preference optimization, reducing the model’s reliance on text biases and enhancing its ability to leverage visual information when answering questions.

Extensive experiments demonstrate that MFPO delivers strong performance on multimodal datasets. Tested on LLaVA-v1.5 models (7B and 13B parameters) and the top-performing LLaVA-v1.6, our method achieved state-of-the-art (SOTA) results on Object HalBench for 7B models, with a CHAIRi score of 5.1, outperforming current methods by nearly 40%. MFPO also achieved SOTA performance on the AMBER dataset, with over a 20% reduction in hallucination rate compared to previous approaches. Additionally, we conducted ablation studies to validate the effectiveness of each module. Our key contributions are: (1) Unlike previous work that primarily focuses on constructing text preference datasets, we address the gap in image preference data construction under multimodal preference optimization. (2) We identified that traditional preference optimization methods often prioritizes text preferences, leading to the neglect of image preference optimization. To resolve this, we propose a joint optimization approach that balances preferences across modalities in MLLMs. (3) Our comprehensive analysis underscores the importance of balanced preference optimization for both text and image in DPO for MLLMs, paving the way for future research in this area.

2 Preliminaries

2.1 Reinforcement Learning from Human Feedback (RLHF)

Reinforcement Learning from Human Feedback (RLHF) aligns models with human preferences using a reward model r_ϕ (Schulman et al., 2017), trained on pairwise preference data (Christiano et al., 2017; Ouyang et al., 2022; Casper et al., 2023). The model assigns higher rewards to preferred outputs, with the cross-entropy loss:

$$L_{RM} = -\log (\sigma (r_\phi(x, y_w) - r_\phi(x, y_l))), \quad (1)$$

where $\sigma(\cdot)$ is the logistic sigmoid, and $r_\phi(x, y_w)$ and $r_\phi(x, y_l)$ represent the rewards for the preferred and less preferred outputs.

After training, the policy π_θ is optimized by maximizing the expected reward while regularizing it to prevent divergence from the reference policy π_{ref} ,

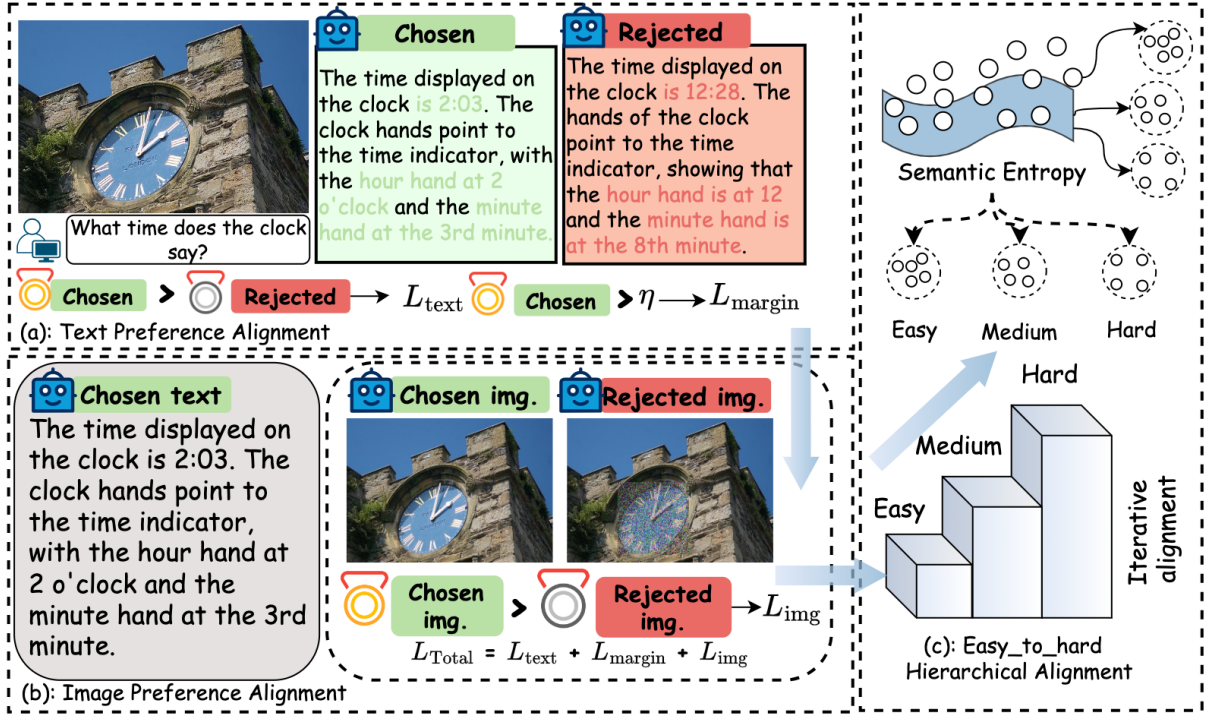


Figure 2: Overview of the MFPO framework. (a) Chosen and rejected text responses are compared to compute text loss L_{text} , with margin loss L_{margin} for reward stability. (b) Chosen and perturbed rejected images are compared, optimizing image preferences with loss L_{img} . (c) Samples are categorized by difficulty using semantic entropy, facilitating progressive training. The total loss L_{Total} combines L_{text} , L_{margin} , and L_{img} .

using a KL divergence penalty:

$$\max_{\pi_\theta} \mathbb{E}_{x \sim D, y \sim \pi_\theta(y|x)} [r_\phi(x, y) - \beta D_{KL}(\pi_\theta(y|x) \parallel \pi_{ref}(y|x))], \quad (2)$$

where β balances reward maximization and regularization. The KL divergence ensures policy stability (Peng et al., 2023; Zhu et al., 2024).

2.2 Direct Preference Optimization (DPO)

DPO directly optimizes a policy π_θ using preference data D (Rafailov et al., 2024), without relying on a reward model. Concretely, DPO derives a theoretical mapping between the reward $r(x, y)$ and the policy π_θ , given by:

$$r(x, y) = \beta \log \frac{\pi_\theta(y|x)}{\pi_{ref}(y|x)} + \beta \log Z(x), \quad (3)$$

where $Z(x)$ is the partition function, defined as $Z(x) = \sum_y \pi_{ref}(y|x) \exp\left(\frac{1}{\beta} r(x, y)\right)$. Substitute Eq. 3 into Eq. 1, we can derive the following loss:

$$L_{DPO}(\pi_\theta; \pi_{sft}) = -\mathbb{E}_{(x, y_w, y_l) \sim D} \left[\log \sigma \left(\beta \log \frac{\pi_\theta(y_w|x)}{\pi_{sft}(y_w|x)} - \beta \log \frac{\pi_\theta(y_l|x)}{\pi_{sft}(y_l|x)} \right) \right], \quad (4)$$

where y_w and y_l denote the preferred and less preferred outputs, respectively. This approach bypasses the complexity of RLHF by allowing the

policy gradient to be computed analytically, ensuring efficient alignment with human preferences (Xu et al., 2024; Feng et al., 2024a).

The common approach in DPO for MLLMs (Yu et al., 2024a,b; Sun et al., 2023; Zhou et al., 2024) involves concatenating the image m and question t into a single input x , followed by optimization using Eq. 4. Chosen responses y_w typically provide accurate, hallucination-free information, while rejected responses y_l often contain hallucinated details, making them less preferred.

3 Modality-Fair Preference Optimization

3.1 Image Preference Data Generation

We introduce the construction of our image preference data as shown in Figure 3. A key question is: *what defines effective image preference data in DPO for MLLMs?* Previous works on text preference data (Pal et al., 2024; Chen et al., 2024a; Gou and Nguyen, 2024) suggest that optimal preference data consists of chosen and rejected responses with moderate differences, as this balance enhances gradient effectiveness during training and helps the model capture subtle content distinctions. Inspired by this, our approach focuses on generating image

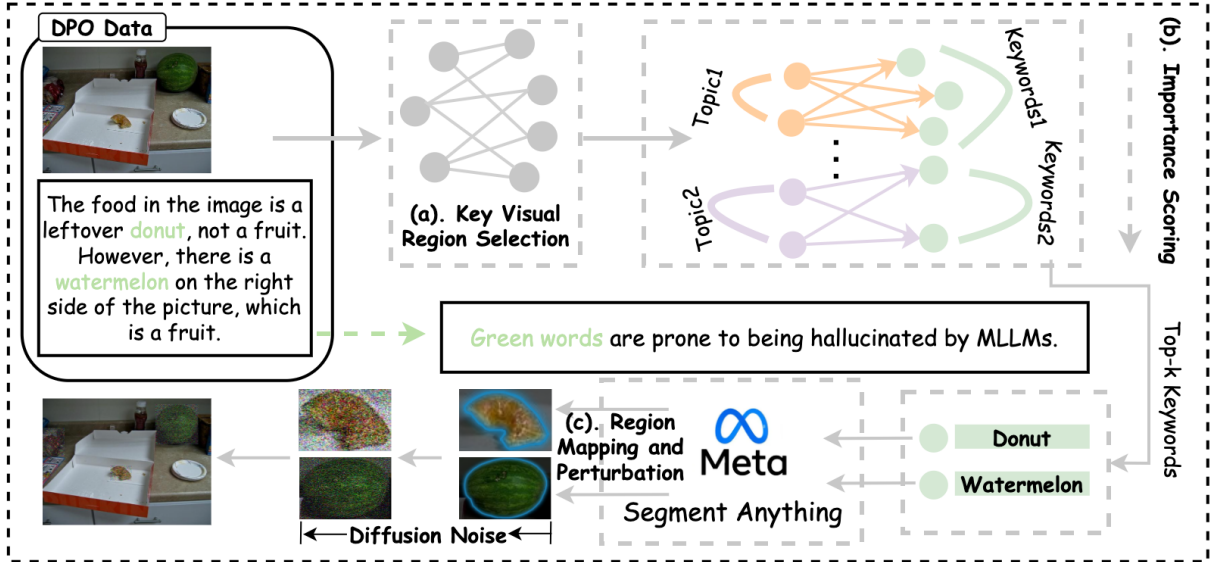


Figure 3: Our data generation pipeline consists of three stages: (a) Key Visual Region Selection, where important image regions are identified using a multipartite graph to extract keywords from preference data; (b) Importance Scoring, ranking the keywords to select the top- k ; and (c) Region Mapping and Perturbation, where selected regions are perturbed with diffusion noise to generate rejected images.

preference data with fine-grained variation, which involves introducing perturbations only to the key regions of the original image most relevant to the chosen responses.

Key Visual Region Selection: To achieve balanced optimization of image and text preferences, we refine the construction of image preference data at the region level to better capture image preferences. Given the complexity of relationships within the text, using a graph-based approach allows us to capture intricate connections between sentences more effectively. Thus, we extract keywords from the text using a multipartite graph approach (Jin and Zhang, 2014; Boudin, 2018; Dawande et al., 2001). We construct a graph $G = (V, E)$, where nodes V represent keywords and edges E encode both positional and semantic relationships. The positional influence between two keywords k_i and k_j is defined as $\theta_{ij} = \sum_{l_i \in \mathcal{L}(k_i)} \sum_{l_j \in \mathcal{L}(k_j)} \frac{1}{1 + |l_i - l_j|^\beta}$, where β controls the decay with distance. Semantic similarity is calculated using cosine similarity: $S(k_i, k_j) = \frac{\mathbf{v}(k_i) \cdot \mathbf{v}(k_j)}{\|\mathbf{v}(k_i)\| \|\mathbf{v}(k_j)\|}$, and the edge weight is a combination of positional and semantic factors: $\mu_{ij} = \theta_{ij} + \sigma_{ij}$, with $\sigma_{ij} = \gamma \cdot S(k_i, k_j)$. We further refine these relationships by adjusting edge weights contextually using related keywords and apply positional decay $\kappa_{ij} = e^{-\lambda l_i}$ to emphasize proximity. The final edge weight $\omega_{ij} = \tau_{ij} \cdot \kappa_{ij}$ integrates positional, semantic, and contextual factors.

Importance Scoring: Since different regions

in an image hold varying significance, focusing on critical regions allows the model to prioritize these areas during preference optimization. To achieve this, we rank the keywords k_i accordingly. Once the graph is constructed, we compute a ranking score for each keyword based on its centrality using a weighted PageRank-inspired algorithm (Bianchini et al., 2005; Haveliwala, 1999; Mihalcea and Tarau, 2004). The initial score for each keyword k_i is $r_0(k_i) = (1 - \alpha)$, where α is a damping factor. The score of each keyword is influenced by its neighbors, with the contribution from a neighboring keyword k_j calculated as $r_{prop}(k_i, k_j) = \frac{\omega_{ij} \cdot r(k_j)}{\sum_{k_m \in \mathcal{N}(k_j)} \omega_{jm}}$, where ω_{ij} is the edge weight, $r(k_j)$ is the neighbor's score, and $\mathcal{N}(k_j)$ represents the neighbors of k_j . The score for each keyword k_i is updated iteratively using $r(k_i) = (1 - \alpha) + \alpha \cdot \sum_{k_j \in \mathcal{N}(k_i)} r_{prop}(k_i, k_j)$, with α controlling the influence of neighbors. This process continues until convergence, at which point the keywords are ranked by their final scores $r(k_i)$. The top k keywords, representing the most significant regions in the image, are then selected.

Region Mapping and Perturbation: When extracting keywords from text preference data, these typically correspond to the regions most prone to hallucinations, making it crucial to identify their corresponding image regions to ensure that image preference optimization also focuses on these key areas. The top-ranked keywords guide a modified

Segment Anything Model (SAM) (Kirillov et al., 2023), mapping each keyword k_i to its corresponding visual region. We then apply diffusion noise to perturb these regions (Ho et al., 2020; Kassam, 2012; Russo, 2003). For each region R_i of the image m , the perturbation follows the diffusion process $m' = \sqrt{\alpha_t} \cdot R_i + \sqrt{1 - \alpha_t} \cdot \eta$, where $\alpha_t = \prod_{j=0}^t \beta_j$ (with $\beta_t \in (0, 1)$ as a hyperparameter controlling the noise schedule), and η is random noise sampled from a standard normal distribution. This perturbation selectively distorts key regions, encouraging the model to focus on critical areas. For keywords that cannot be mapped to visual regions, we apply a global regularization method, adding diffusion noise to all image regions, thus generating rejected image data. These perturbed images m' serve as rejected preference images in Direct Preference Optimization (DPO), refining the model’s alignment with fine-grained visual details.

3.2 MFPO Training Process

We leverage the image preference data generated in earlier steps, enabling unified optimization of the policy π_θ across both text and image modalities.

Text Preference Alignment: The DPO policy objective for text preference optimization is expressed as:

$$L_{\text{text}}(\pi_\theta; \pi_{\text{ref}}) = -\mathbb{E}_D \left[\log \sigma \left(\beta \log \frac{\pi_\theta(y_w|t, m)}{\pi_{\text{ref}}(y_w|t, m)} \right) - \log \sigma \left(\beta \log \frac{\pi_\theta(y_l|t, m)}{\pi_{\text{ref}}(y_l|t, m)} \right) \right], \quad (5)$$

where t and m represents the original text and image inputs. y_w and y_l are the preferred and less preferred outputs. π_{ref} is the reference policy.

Image Preference Alignment: For image preference optimization, we use the original image m and the perturbed image m' generated in earlier steps. The image preference loss is defined as:

$$L_{\text{image}}(\pi_\theta; \pi_{\text{ref}}) = -\mathbb{E}_D \left[\log \sigma \left(\beta \log \frac{\pi_\theta(y_w|t, m)}{\pi_{\text{ref}}(y_w|t, m)} \right) - \log \sigma \left(\beta \log \frac{\pi_\theta(y_w|t, m')}{\pi_{\text{ref}}(y_w|t, m')} \right) \right]. \quad (6)$$

Note that we only use the preferred response y_w for image preference alignment.

Margin Loss for Stability: To address potential instability during the joint optimization of text and image preferences, we introduce a margin loss to penalize situations where both chosen and rejected responses experience a reduction in reward, drawing inspiration from previous research (Meng et al.,

2024; Chen et al., 2024a; Wang et al., 2024). The margin loss is defined as:

$$L_{\text{margin}} = -\log \sigma \left(\beta \log \frac{\pi_\theta(y_w|t, m)}{\pi_{\text{ref}}(y_w|t, m)} - \eta \right), \quad (7)$$

where η is the margin parameter that enforces a greater separation between positive (chosen) and negative (rejected) responses. The total loss for the training phase is defined as $L_{\text{total}} = L_{\text{text}} + L_{\text{image}} + L_{\text{margin}}$, ensuring that both text and image preferences are jointly optimized while maintaining stability in their alignment.

3.3 Easy-to-Hard Iterative Alignment

We introduce an Easy-to-Hard Iterative Alignment algorithm to stabilize the training of MFPO (Pal et al., 2024; Sun et al., 2024; Feng et al., 2024b).

Entropy Calculation: Leveraging semantic entropy (Venuhizen et al., 2019; Farquhar et al., 2024), we estimate the uncertainty of the model’s responses. Given a probability distribution of predicted answers $P = \{p_1, p_2, \dots, p_n\}$, where p_i represents the probability of the i -th predicted token, the entropy H is calculated as $H(P) = -\sum_{i=1}^n p_i \log(p_i)$. This measure quantifies the uncertainty inherent in the model’s predictions.

Sorting by Difficulty: After calculating entropy for all training samples, we rank the training dataset according to their entropy scores, where higher values denoting more challenging inputs. We then divide the dataset into three distinct difficulty levels: easy, medium, and hard.

Iterative Alignment: By progressively moving from easy to hard examples, the feedback distribution is iteratively updated. This ensures that the model first learns simpler patterns and builds a foundation before tackling more complex cases. As the training progresses, the alignment becomes more refined, allowing the model to effectively handle harder examples.

4 Experiments

4.1 Experimental Setup

Implementation Details. We use LLaVA-v1.5 as the backbone for all experiments and include the latest top-performing LLaVA-v1.6 to validate the generalization of our method. The training consists of three stages: the first two stages follow standard LLaVA training, while DPO is introduced in the third stage. Here, we construct image preference data based on Section 3.1, using text preference

Methods	MMHalBench		Object HalBench			AMBER		
	Score \uparrow	HalRate \downarrow	CHAIR _s \downarrow	CHAIR _i \downarrow	CHAIR _s \downarrow	Cover. \uparrow	HalRate \downarrow	Cog. \downarrow
Referenced Results								
7B MLLMs								
LLaVA-v1.6-7B (Liu et al., 2024b)	2.46	0.52	16.4	9.4	9.1	61.7	50.2	4.7
LLaVA-v1.5-7B (Liu et al., 2024b)	2.07	0.59	53.6	25.2	7.8	51.0	36.4	4.2
+ HACL (Jiang et al., 2024a)	2.13	0.50	—	—	—	—	—	—
+ Povid (Zhou et al., 2024)	2.08	0.56	48.1	24.4	—	—	—	—
+ OPERA (Huang et al., 2024a)	2.15	0.54	45.1	22.3	—	—	—	—
+ VCD (Leng et al., 2024)	2.04	0.58	48.0	22.3	—	—	—	—
+ DPO (Rafailov et al., 2024)	2.14	0.65	49.0	13.0	6.5	55.5	34.5	2.3
+ mDPO (Wang et al., 2024)	2.39	0.54	35.7	9.8	4.4	52.4	24.5	2.4
+ EOS (Yue et al., 2024)	2.03	0.59	40.3	17.8	5.1	49.1	22.7	2.0
+ HA-DPO (Zhao et al., 2023b)	1.97	0.59	39.9	19.9	6.7	49.8	30.9	3.3
+ HALVA (Sarkar et al., 2024)	2.08	0.60	46.6	53.0	6.6	53.0	33.2	3.4
LLaVA-v1.5-7B + MFPO	2.69	0.49	13.4	6.6	4.1	55.7	22.5	1.9
LLaVA-v1.6-7B + MFPO	2.89	0.45	10.6	5.1	3.1	58.8	18.7	1.1
>=13B MLLMs								
GPT-4V (Achiam et al., 2023)	3.49	0.28	13.6	7.3	4.6	67.1	30.7	2.6
MiniGemini-34B (Li et al., 2024)	3.08	0.38	14.5	8.0	—	—	—	—
Qwen-VL-Chat (Bai et al., 2023)	2.89	0.43	36.0	21.3	6.6	53.2	31.0	2.9
LLaVA-v1.5-13B (Liu et al., 2024a)	2.42	—	46.3	22.6	7.8	51.0	36.4	4.2
+ RLHF-V (Yu et al., 2024a)	2.81	0.49	12.2	7.5	6.3	46.1	25.1	2.1
+ HSA-DPO (Xiao et al., 2024)	2.61	0.48	5.2	3.2	2.1	47.3	13.4	1.2
+ HALVA (Sarkar et al., 2024)	2.84	0.48	—	—	6.4	52.6	30.4	3.2
LLaVA-v1.5-13B + MFPO	2.94	0.42	11.4	4.6	3.4	56.1	19.4	1.4

Table 1: Results for MMHalBench, Object HalBench, and AMBER benchmarks.

	overall	attribute	adversarial	comparison	counting	relation	environment	holistic	other
LLaVA-RLHF-7B	2.05	2.92	1.83	2.42	1.92	2.25	2.25	1.75	1.08
LLaVA-RLHF-13B	2.53	3.33	2.67	1.75	2.25	2.33	3.25	2.25	2.42
LLaVA-v1.5-7B	2.07	3.08	1.08	2.58	2.25	2.0	3.0	1.42	1.33
+ MFPO	2.69	3.33	3.67	2.42	2.25	2.75	3.42	2.00	1.83

Table 2: Performance comparison across different dimensions in MMHalBench

data from RLHF-V (Yu et al., 2024a), and apply MFPO optimization. To accelerate training, we use LoRA with $r = 128$ and set the learning rate to $2e^{-5}$ over three epochs, following prior work (Yu et al., 2024b; Zhou et al., 2024; Wang et al., 2024).

Evaluation. We conducted a comprehensive evaluation using a range of benchmarks. Object HalBench (Rohrbach et al., 2018) was used to assess common object hallucinations in image descriptions, with CHAIR scores for both response-level (CHAIRs) and object-level (CHAIRi) hallucination rates. MMHal-Bench (Sun et al., 2023) measured response quality and hallucination rates by comparing model outputs with human responses and object labels. Additionally, AMBER (Wang et al., 2023) evaluated generative tasks, providing metrics on CHAIR variants, object coverage, and cognitive hallucination rates. Details in Appendix A.1

Baselines. We compare our model with state-of-the-art baselines across multiple categories.

For general MLLMs, we include LLaVA1.5 (Liu et al., 2024a), Qwen-VL-Chat (Bai et al., 2023), LLaVA1.6, and MiniGemini (Li et al., 2024). We also compare with preference-feedback models such as Povid (Zhou et al., 2024), RLHF-V (Yu et al., 2024a), and Silkie (Sun et al., 2023), as well as feedback-independent methods like VCD (Leng et al., 2024). Additionally, we benchmark against GPT-4V (Achiam et al., 2023), a proprietary model. Details in Appendix A.2

4.2 Main Results

Comparison to Existing Methods. The main results are shown in Table 1. After integrating MFPO, both LLaVA-v1.5 and LLaVA-v1.6 consistently improve across all three datasets, significantly reducing hallucinations and enhancing trustworthiness. Notably, on Object HalBench, our method surpasses GPT-4V in trustworthiness for both models. Additionally, on MMHalBench and Object

HalBench, our approach achieves state-of-the-art performance among all 7B-parameter models. This demonstrates that MFPO’s balance of text and image modality optimization leads to superior trustworthiness and highlights the importance of modality balance for robust performance. As shown in Table 2, our method improves performance across all evaluation dimensions, indicating a comprehensive enhancement of MLLM trustworthiness.

Weak-to-Strong Trustworthiness Improvements. Comparing MFPO with the 7B LLaVA-v1.5 model to larger models like LLaVA-v1.5-13B and MiniGemini-34B, we find that MFPO, by performing fair preference optimization across both text and image modalities, enables the smaller 7B model to match or even surpass the trustworthiness of the 13B and 34B models. This demonstrates that MFPO significantly enhances trustworthiness in smaller models, balancing optimizations across modalities while maintaining scalability.

4.3 Ablation Study and Analysis

L_{text}	L_{image}	L_{margin}	MMHalBench		Object HalBench	
			Score \uparrow	HalRate \downarrow	CHAIR _s \downarrow	CHAIR _i \downarrow
✓	x	✓	2.46	0.53	21.9	10.9
x	✓	✓	2.34	0.56	24.4	13.1
✓	✓	x	2.61	0.50	16.9	7.9
✓	✓	✓	2.69	0.49	13.4	6.6

Table 3: Ablation study of different loss compositions.

Ablation of Different Loss Compositions. We conduct experiments to validate the loss composition in MFPO. As shown in Table 3, optimizing solely on L_{text} improves performance but still has limitations, leading to an over-reliance on text preferences. Conversely, focusing only on the image modality helps address the imbalance between image and text preferences, but the lack of text optimization also limits performance. This underscores the importance of jointly optimizing both text and visual modalities in multimodal tasks. Furthermore, incorporating margin loss not only stabilizes training but also boosts performance slightly. Our ablation study confirms the effectiveness of each loss component in the method.

Training Method	MMHalBench		Object HalBench	
	Score \uparrow	HalRate \downarrow	CHAIR _s \downarrow	CHAIR _i \downarrow
Easy-to-hard	2.69	0.49	13.4	6.6
End-to-end	<u>2.53</u>	<u>0.53</u>	<u>16.0</u>	<u>8.0</u>

Table 4: Comparison of different training methods.

Ablation of Easy-to-Hard Alignment Scheme.

We validate the effectiveness of the easy-to-hard alignment scheme by comparing it with training on all data simultaneously. As shown in Table 4, our method consistently outperforms the traditional approach. Figure 5 highlights the greater stability provided by the easy-to-hard strategy. Starting with easier preference data allows the model to establish a better optimization direction early on, resulting in more stable improvements when processing medium and hard data. This confirms the effectiveness of our iterative alignment method.

Construction Method	MMHalBench		Object HalBench	
	Score \uparrow	HalRate \downarrow	CHAIR _s \downarrow	CHAIR _i \downarrow
Global	<u>2.56</u>	0.56	21.7	10.3
Random 20%	2.45	<u>0.52</u>	<u>16.5</u>	<u>8.5</u>
Ours	2.69	0.49	13.4	6.6

Table 5: Comparison of different image preference data construction.

Ablation of Different Image Preference Data Construction.

We conduct experiments to explore how varying levels of noise granularity and proportions affect the balance of preference optimization. Specifically, we compare three methods for constructing image preference data: applying global diffusion noise to the entire image, adding diffusion noise to 20% of randomly selected image areas, and our fine-grained diffusion noise addition approach. As shown in Table 5, constructing image preference data encourages the model to focus on image-based optimization during preference alignment. However, as the granularity of the image preference data becomes coarser, the model’s optimization shifts more toward text preferences, resulting in suboptimal performance. Coarse-grained image preference data construction leads to overly simplistic optimization of image features, preventing the model from effectively aligning preferences for image content related to the text.

Effect of Key Visual Region Selection. To verify the accuracy of extracting key visual keyphrases from the original text preference data using a multipartite graph, we randomly sample 100 examples and check their correctness. We find that 81% of the samples correspond to important objects in the associated preference data. In 19% of the cases, although the keyphrases are extracted, SAM does not correctly mask them. However, our method mitigates this issue by adding diffusion noise to the entire image, reducing the impact of such cases on performance.

Method	Conversation	Captioning
LLaVA-1.5	53.3	53.4
+ VIfeedback	51.3	49.3
+ Human-Preference	49.6	43.3
+ RLHF-V	<u>55.8</u>	<u>56.1</u>
Ours	65.8	60.0

Table 6: Comparison of different methods across conversation and captioning performance.

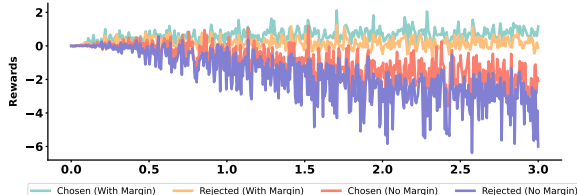


Figure 4: Rewards comparasion

Fine-grained Perception Improvement. To verify whether our visual enhanced DPO can enhance the fine-grained perception capability of MLLM, we analyze different preference collection strategies on the LLaVA-Bench benchmark. We focus on the performance related to conversation and detailed descriptions, which represent fine-grained perception abilities. As shown in Table 6, our method outperforms both LLaVA-v1.5 and other alignment methods, indicating that our approach not only reduces visual hallucinations and enhances trustworthiness but also improves the overall perception capability of the model.

Margin	MMHalBench		Object HalBench	
	Score \uparrow	HalRate \downarrow	CHAIR _s \downarrow	CHAIR _i \downarrow
0 (Ours)	2.69	0.49	13.4	6.6
0.2	2.58	0.50	15.7	7.1
0.4	<u>2.63</u>	0.52	16.0	7.9

Table 7: Comparison of different margin.

Margin	MMHalBench		Object HalBench	
	Score \uparrow	HalRate \downarrow	CHAIR _s \downarrow	CHAIR _i \downarrow
easy	2.37	0.55	24.1	13.1
medium	<u>2.55</u>	<u>0.53</u>	<u>17.3</u>	<u>9.1</u>
hard	2.69	0.49	13.4	6.6

Table 8: Each stage’s performance

Margin Loss Improves Stability. We analyze the benefits that margin loss brings to preference optimization training. During convergence, both chosen and rejected responses can experience si-

multaneous decreases in rewards. By incorporating margin loss, we penalize reductions in rewards for chosen responses. As shown in Figure 4, reward changes during training become more stable, highlighting the role of margin loss in improving training stability. Additionally, as shown in Table 7, margins of 0, 0.2, and 0.4 all improve model performance, with a margin of 0 yielding the best results, further validating the importance of margin loss. Moreover, small margin settings maintain both performance and training stability.

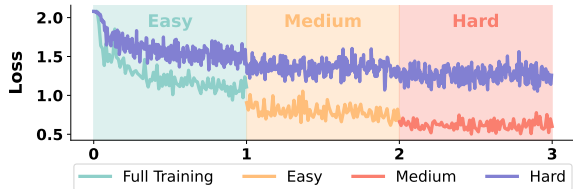


Figure 5: Loss comparasion

Effect of Easy-to-Hard Training Strategy. Beyond performance comparisons, we analyze the easy-to-hard DPO training approach against the traditional full training paradigm. As shown in Figure 5, the easy-to-hard strategy achieves better convergence, with the loss decreasing more rapidly during the easy phase, indicating quick alignment learning. As training samples become more difficult, the loss reduction slows, allowing the model to learn finer-grained knowledge from challenging samples. Moreover, the increasing loss differences across difficulty stages demonstrate that this strategy enables the model to gain more from harder samples compared to traditional training, making it a more stable and efficient training method.

5 Conclusion

We proposed Modality-Fair Preference Optimization (MFPO) to address the bias toward text in multimodal large language models (MLLMs) using DPO, which often leads to visual hallucinations. By incorporating fine-grained image preference data and balancing optimization between text and image, MFPO improves model trustworthiness. Our multi-stage alignment strategy further stabilizes training. Experiments show that MFPO significantly reduces hallucinations and achieves state-of-the-art performance on benchmarks like Object HalBench and AMBER. Moreover, MFPO demonstrates the importance of modality balance in multimodal tasks, ensuring the model leverages both

visual and textual information effectively. This balanced approach not only improves model reliability but also enhances its interpretability in complex visual reasoning tasks. Our results highlight the potential of MFPO to set a new standard for preference optimization in MLLMs, paving the way for more robust and trustworthy models.

6 Limitations

Our work also has limitations. First, the effectiveness of our method on larger models with greater parameter counts remains unclear. Once we have access to more powerful computing resources, we will conduct experiments to validate our approach on models of larger scales. Additionally, the datasets available for evaluating model trustworthiness are currently limited. We require more diverse datasets to thoroughly assess the effectiveness of our method across multiple dimensions.

References

Josh Achiam, Steven Adler, Sandhini Agarwal, Lama Ahmad, Ilge Akkaya, Florencia Leoni Aleman, Diogo Almeida, Jankó Altenschmidt, Sam Altman, Shyamal Anadkat, et al. 2023. Gpt-4 technical report. *arXiv preprint arXiv:2303.08774*.

Elmira Amirloo, Jean-Philippe Fauconnier, Christoph Roesmann, Christian Kerl, Rinu Boney, Yusu Qian, Zirui Wang, Afshin Dehghan, Yinfei Yang, Zhe Gan, et al. 2024. Understanding alignment in multi-modal llms: A comprehensive study. *arXiv preprint arXiv:2407.02477*.

Jinze Bai, Shuai Bai, Shusheng Yang, Shijie Wang, Sinan Tan, Peng Wang, Junyang Lin, Chang Zhou, and Jingren Zhou. 2023. Qwen-vl: A versatile vision-language model for understanding, localization, text reading, and beyond.

Yuntao Bai, Andy Jones, Kamal Ndousse, Amanda Askell, Anna Chen, Nova DasSarma, Dawn Drain, Stanislav Fort, Deep Ganguli, Tom Henighan, et al. 2022. Training a helpful and harmless assistant with reinforcement learning from human feedback. *arXiv preprint arXiv:2204.05862*.

Zechen Bai, Pichao Wang, Tianjun Xiao, Tong He, Zongbo Han, Zheng Zhang, and Mike Zheng Shou. 2024. Hallucination of multimodal large language models: A survey. *arXiv preprint arXiv:2404.18930*.

Yoshua Bengio, Jérôme Louradour, Ronan Collobert, and Jason Weston. 2009. Curriculum learning. In *Proceedings of the 26th annual international conference on machine learning*, pages 41–48.

Monica Bianchini, Marco Gori, and Franco Scarselli. 2005. Inside pagerank. *ACM Transactions on Internet Technology (TOIT)*, 5(1):92–128.

Florian Boudin. 2018. Unsupervised keyphrase extraction with multipartite graphs. *arXiv preprint arXiv:1803.08721*.

Stephen Casper, Xander Davies, Claudia Shi, Thomas Krendl Gilbert, Jérémie Scheurer, Javier Rando, Rachel Freedman, Tomasz Korbak, David Lindner, Pedro Freire, et al. 2023. Open problems and fundamental limitations of reinforcement learning from human feedback. *arXiv preprint arXiv:2307.15217*.

Huayu Chen, Guande He, Hang Su, and Jun Zhu. 2024a. Noise contrastive alignment of language models with explicit rewards. *arXiv preprint arXiv:2402.05369*.

Long Chen, Xin Yan, Jun Xiao, Hanwang Zhang, Shiliang Pu, and Yueting Zhuang. 2020. Counterfactual samples synthesizing for robust visual question answering. In *Proceedings of the IEEE/CVF conference on computer vision and pattern recognition*, pages 10800–10809.

Ruizhe Chen, Jianfei Yang, Huimin Xiong, Jianhong Bai, Tianxiang Hu, Jin Hao, Yang Feng, Joey Tianyi Zhou, Jian Wu, and Zuozhu Liu. 2024b. Fast model debias with machine unlearning. *Advances in Neural Information Processing Systems*, 36.

Ruizhe Chen, Xiaotian Zhang, Meng Luo, Wenhao Chai, and Zuozhu Liu. 2024c. Pad: Personalized alignment at decoding-time. *arXiv preprint arXiv:2410.04070*.

Paul F Christiano, Jan Leike, Tom Brown, Miljan Martic, Shane Legg, and Dario Amodei. 2017. Deep reinforcement learning from human preferences. *Advances in neural information processing systems*, 30.

Milind Dawande, Pinar Keskinocak, Jayashankar M Swaminathan, and Sridhar Tayur. 2001. On bipartite and multipartite clique problems. *Journal of Algorithms*, 41(2):388–403.

Sebastian Farquhar, Jannik Kossen, Lorenz Kuhn, and Yarin Gal. 2024. Detecting hallucinations in large language models using semantic entropy. *Nature*, 630(8017):625–630.

Alessandro Favero, Luca Zancato, Matthew Trager, Siddharth Choudhary, Pramuditha Perera, Alessandro Achille, Ashwin Swaminathan, and Stefano Soatto. 2024. Multi-modal hallucination control by visual information grounding. In *Proceedings of the IEEE/CVF Conference on Computer Vision and Pattern Recognition*, pages 14303–14312.

Duanyu Feng, Bowen Qin, Chen Huang, Zheng Zhang, and Wenqiang Lei. 2024a. Towards analyzing and understanding the limitations of dpo: A theoretical perspective. *arXiv preprint arXiv:2404.04626*.

Zhaopeng Feng, Ruizhe Chen, Yan Zhang, Zijie Meng, and Zuozhu Liu. 2024b. Ladder: A model-agnostic framework boosting llm-based machine translation to the next level. *arXiv preprint arXiv:2406.15741*.

Qi Gou and Cam-Tu Nguyen. 2024. Mixed preference optimization: Reinforcement learning with data selection and better reference model. *arXiv preprint arXiv:2403.19443*.

Taher Haveliwala. 1999. Efficient computation of pagerank. Technical report, Stanford.

Jonathan Ho, Ajay Jain, and Pieter Abbeel. 2020. Denoising diffusion probabilistic models. *Advances in neural information processing systems*, 33:6840–6851.

Qidong Huang, Xiaoyi Dong, Pan Zhang, Bin Wang, Conghui He, Jiaqi Wang, Dahua Lin, Weiming Zhang, and Nenghai Yu. 2024a. Opera: Alleviating hallucination in multi-modal large language models via over-trust penalty and retrospection-allocation. In *Proceedings of the IEEE/CVF Conference on Computer Vision and Pattern Recognition*, pages 13418–13427.

Wen Huang, Hongbin Liu, Minxin Guo, and Neil Zhenqiang Gong. 2024b. Visual hallucinations of multi-modal large language models. *arXiv preprint arXiv:2402.14683*.

Chaoya Jiang, Haiyang Xu, Mengfan Dong, Jiaxing Chen, Wei Ye, Ming Yan, Qinghao Ye, Ji Zhang, Fei Huang, and Shikun Zhang. 2024a. Hallucination augmented contrastive learning for multimodal large language model. In *Proceedings of the IEEE/CVF Conference on Computer Vision and Pattern Recognition*, pages 27036–27046.

Songtao Jiang, Yan Zhang, Chenyi Zhou, Yeying Jin, Yang Feng, Jian Wu, and Zuozhu Liu. 2024b. Joint visual and text prompting for improved object-centric perception with multimodal large language models. *arXiv preprint arXiv:2404.04514*.

Ya-Lei Jin and Xiao-Dong Zhang. 2014. Complete multipartite graphs are determined by their distance spectra. *Linear Algebra and its Applications*, 448:285–291.

Chenchen Jing, Yuwei Wu, Xiaoxun Zhang, Yunde Jia, and Qi Wu. 2020. Overcoming language priors in vqa via decomposed linguistic representations. In *Proceedings of the AAAI conference on artificial intelligence*, volume 34, pages 11181–11188.

Jean Kaddour, Joshua Harris, Maximilian Mozes, Herbie Bradley, Roberta Raileanu, and Robert McHardy. 2023. Challenges and applications of large language models. *arXiv preprint arXiv:2307.10169*.

Saleem A Kassam. 2012. *Signal detection in non-Gaussian noise*. Springer Science & Business Media.

Alexander Kirillov, Eric Mintun, Nikhila Ravi, Hanzi Mao, Chloe Rolland, Laura Gustafson, Tete Xiao, Spencer Whitehead, Alexander C Berg, Wan-Yen Lo, et al. 2023. Segment anything. In *Proceedings of the IEEE/CVF International Conference on Computer Vision*, pages 4015–4026.

Sicong Leng, Hang Zhang, Guanzheng Chen, Xin Li, Shijian Lu, Chunyan Miao, and Lidong Bing. 2024. Mitigating object hallucinations in large vision-language models through visual contrastive decoding. In *Proceedings of the IEEE/CVF Conference on Computer Vision and Pattern Recognition*, pages 13872–13882.

Yanwei Li, Yuechen Zhang, Chengyao Wang, Zhisheng Zhong, Yixin Chen, Ruihang Chu, Shaoteng Liu, and Jiaya Jia. 2024. Mini-gemini: Mining the potential of multi-modality vision language models. *arXiv preprint arXiv:2403.18814*.

Yicong Li, Xiang Wang, Junbin Xiao, Wei Ji, and Tat-Seng Chua. 2022. Invariant grounding for video question answering. In *Proceedings of the IEEE/CVF Conference on Computer Vision and Pattern Recognition*, pages 2928–2937.

Zujie Liang, Weitao Jiang, Haifeng Hu, and Jiaying Zhu. 2020. Learning to contrast the counterfactual samples for robust visual question answering. In *Proceedings of the 2020 conference on empirical methods in natural language processing (EMNLP)*, pages 3285–3292.

Haotian Liu, Chunyuan Li, Yuheng Li, and Yong Jae Lee. 2024a. Improved baselines with visual instruction tuning. In *Proceedings of the IEEE/CVF Conference on Computer Vision and Pattern Recognition*, pages 26296–26306.

Haotian Liu, Chunyuan Li, Qingyang Wu, and Yong Jae Lee. 2024b. Visual instruction tuning. *Advances in neural information processing systems*, 36.

Yang Liu, Yuanshun Yao, Jean-Francois Ton, Xiaoying Zhang, Ruocheng Guo, Hao Cheng, Yegor Klochkov, Muhammad Faaiz Taufiq, and Hang Li. 2023. Trustworthy llms: A survey and guideline for evaluating large language models’ alignment. *arXiv preprint arXiv:2308.05374*.

Tambet Matiisen, Avital Oliver, Taco Cohen, and John Schulman. 2019. Teacher–student curriculum learning. *IEEE transactions on neural networks and learning systems*, 31(9):3732–3740.

Yu Meng, Mengzhou Xia, and Danqi Chen. 2024. Simpo: Simple preference optimization with a reference-free reward. *arXiv preprint arXiv:2405.14734*.

Rada Mihalcea and Paul Tarau. 2004. Textrank: Bringing order into text. In *Proceedings of the 2004 conference on empirical methods in natural language processing*, pages 404–411.

Humza Naveed, Asad Ullah Khan, Shi Qiu, Muhammad Saqib, Saeed Anwar, Muhammad Usman, Naveed Akhtar, Nick Barnes, and Ajmal Mian. 2023. A comprehensive overview of large language models. *arXiv preprint arXiv:2307.06435*.

Long Ouyang, Jeffrey Wu, Xu Jiang, Diogo Almeida, Carroll Wainwright, Pamela Mishkin, Chong Zhang, Sandhini Agarwal, Katarina Slama, Alex Ray, et al. 2022. Training language models to follow instructions with human feedback. *Advances in neural information processing systems*, 35:27730–27744.

Arka Pal, Deep Karkhanis, Samuel Dooley, Manley Roberts, Siddartha Naidu, and Colin White. 2024. Smaug: Fixing failure modes of preference optimisation with dpo-positive. *arXiv preprint arXiv:2402.13228*.

Ryan Park, Rafael Rafailov, Stefano Ermon, and Chelsea Finn. 2024. Disentangling length from quality in direct preference optimization. *arXiv preprint arXiv:2403.19159*.

Baolin Peng, Linfeng Song, Ye Tian, Lifeng Jin, Haitao Mi, and Dong Yu. 2023. Stabilizing rlhf through advantage model and selective rehearsal. *arXiv preprint arXiv:2309.10202*.

Renjie Pi, Tiannyang Han, Wei Xiong, Jipeng Zhang, Runtao Liu, Rui Pan, and Tong Zhang. 2024. Strengthening multimodal large language model with bootstrapped preference optimization. *arXiv preprint arXiv:2403.08730*.

Rafael Rafailov, Archit Sharma, Eric Mitchell, Christopher D Manning, Stefano Ermon, and Chelsea Finn. 2024. Direct preference optimization: Your language model is secretly a reward model. *Advances in Neural Information Processing Systems*, 36.

Sainandan Ramakrishnan, Aishwarya Agrawal, and Stefan Lee. 2018. Overcoming language priors in visual question answering with adversarial regularization. *Advances in Neural Information Processing Systems*, 31.

Anna Rohrbach, Lisa Anne Hendricks, Kaylee Burns, Trevor Darrell, and Kate Saenko. 2018. Object hallucination in image captioning. *arXiv preprint arXiv:1809.02156*.

Fabrizio Russo. 2003. A method for estimation and filtering of gaussian noise in images. *IEEE Transactions on Instrumentation and Measurement*, 52(4):1148–1154.

Pritam Sarkar, Sayna Ebrahimi, Ali Etemad, Ahmad Beirami, Sercan Ö Arik, and Tomas Pfister. 2024. Mitigating object hallucination via data augmented contrastive tuning. *arXiv preprint arXiv:2405.18654*.

John Schulman, Filip Wolski, Prafulla Dhariwal, Alec Radford, and Oleg Klimov. 2017. Proximal policy optimization algorithms. *arXiv preprint arXiv:1707.06347*.

Meet Shah, Xinlei Chen, Marcus Rohrbach, and Devi Parikh. 2019. Cycle-consistency for robust visual question answering. In *Proceedings of the IEEE/CVF Conference on Computer Vision and Pattern Recognition*, pages 6649–6658.

Nisan Stiennon, Long Ouyang, Jeffrey Wu, Daniel Ziegler, Ryan Lowe, Chelsea Voss, Alec Radford, Dario Amodei, and Paul F Christiano. 2020. Learning to summarize with human feedback. *Advances in Neural Information Processing Systems*, 33:3008–3021.

Zhiqing Sun, Sheng Shen, Shengcao Cao, Haotian Liu, Chunyuan Li, Yikang Shen, Chuang Gan, Liang-Yan Gui, Yu-Xiong Wang, Yiming Yang, et al. 2023. Aligning large multimodal models with factually augmented rlhf. *arXiv preprint arXiv:2309.14525*.

Zhiqing Sun, Longhui Yu, Yikang Shen, Weiyang Liu, Yiming Yang, Sean Welleck, and Chuang Gan. 2024. Easy-to-hard generalization: Scalable alignment beyond human supervision. *arXiv preprint arXiv:2403.09472*.

Noortje J Venhuizen, Matthew W Crocker, and Harm Brouwer. 2019. Semantic entropy in language comprehension. *Entropy*, 21(12):1159.

Bram Wallace, Meihua Dang, Rafael Rafailov, Linqi Zhou, Aaron Lou, Senthil Purushwalkam, Stefano Ermon, Caiming Xiong, Shafiq Joty, and Nikhil Naik. 2024. Diffusion model alignment using direct preference optimization. In *Proceedings of the IEEE/CVF Conference on Computer Vision and Pattern Recognition*, pages 8228–8238.

Fei Wang, Wenxuan Zhou, James Y Huang, Nan Xu, Sheng Zhang, Hoifung Poon, and Muhaoo Chen. 2024. mdpo: Conditional preference optimization for multimodal large language models. *arXiv preprint arXiv:2406.11839*.

Junyang Wang, Yuhang Wang, Guohai Xu, Jing Zhang, Yukai Gu, Haitao Jia, Ming Yan, Ji Zhang, and Jitao Sang. 2023. An llm-free multi-dimensional benchmark for mllms hallucination evaluation. *arXiv preprint arXiv:2311.07397*.

Wenyi Xiao, Ziwei Huang, Leilei Gan, Wanggui He, Haoyuan Li, Zhenlin Yu, Hao Jiang, Fei Wu, and Linchao Zhu. 2024. Detecting and mitigating hallucination in large vision language models via fine-grained ai feedback. *arXiv preprint arXiv:2404.14233*.

Shusheng Xu, Wei Fu, Jiaxuan Gao, Wenjie Ye, Weilin Liu, Zhiyu Mei, Guangju Wang, Chao Yu, and Yi Wu. 2024. Is dpo superior to ppo for llm alignment? a comprehensive study. *arXiv preprint arXiv:2404.10719*.

Tianyu Yu, Yuan Yao, Haoye Zhang, Taiwen He, Yifeng Han, Ganqu Cui, Jinyi Hu, Zhiyuan Liu, Hai-Tao Zheng, Maosong Sun, et al. 2024a. Rlhf-v: Towards

trustworthy mllms via behavior alignment from fine-grained correctional human feedback. In *Proceedings of the IEEE/CVF Conference on Computer Vision and Pattern Recognition*, pages 13807–13816.

Tianyu Yu, Haoye Zhang, Yuan Yao, Yunkai Dang, Da Chen, Xiaoman Lu, Ganqu Cui, Taiwen He, Zhiyuan Liu, Tat-Seng Chua, et al. 2024b. Rlaif-v: Aligning mllms through open-source ai feedback for super gpt-4v trustworthiness. *arXiv preprint arXiv:2405.17220*.

Zihao Yue, Liang Zhang, and Qin Jin. 2024. Less is more: Mitigating multimodal hallucination from an eos decision perspective. *arXiv preprint arXiv:2402.14545*.

Duzhen Zhang, Yahan Yu, Chenxing Li, Jiahua Dong, Dan Su, Chenhui Chu, and Dong Yu. 2024. Mm-Ilms: Recent advances in multimodal large language models. *arXiv preprint arXiv:2401.13601*.

Mengxi Zhang and Kang Rong. 2024. Automated multi-level preference for mllms. *arXiv preprint arXiv:2405.11165*.

Wayne Xin Zhao, Kun Zhou, Junyi Li, Tianyi Tang, Xiaolei Wang, Yupeng Hou, Yingqian Min, Beichen Zhang, Junjie Zhang, Zican Dong, et al. 2023a. A survey of large language models. *arXiv preprint arXiv:2303.18223*.

Zhiyuan Zhao, Bin Wang, Linke Ouyang, Xiaoyi Dong, Jiaqi Wang, and Conghui He. 2023b. Beyond hallucinations: Enhancing lylms through hallucination-aware direct preference optimization. *arXiv preprint arXiv:2311.16839*.

Jonathan Zhou. 2024. Gamelabel-10k: Collecting image preference data through mobile game crowdsourcing. *arXiv preprint arXiv:2409.19830*.

Yiyang Zhou, Chenhang Cui, Rafael Rafailov, Chelsea Finn, and Huaxiu Yao. 2024. Aligning modalities in vision large language models via preference finetuning. *arXiv preprint arXiv:2402.11411*.

Banghua Zhu, Michael I Jordan, and Jiantao Jiao. 2024. Iterative data smoothing: Mitigating reward overfitting and overoptimization in rlhf. *arXiv preprint arXiv:2401.16335*.

A Example Appendix

A.1 Evaluation Details

For a comprehensive evaluation, we selected a broad set of benchmarks. Object Hal-Bench (Rohrbach et al., 2018) is a standard dataset designed to assess common object hallucinations in image descriptions. We followed (Yu et al., 2024a) and employed 8 diverse prompts to ensure robust evaluation, reporting both response-level (CHAIRs) and object-level (CHAIRi) hallucination rates. Next, we utilized MMHal-Bench (Sun et al., 2023), which measures response quality on a scale of 0-6 and hallucination rates by comparing model outputs with human-generated responses and object labels. This allows for a detailed understanding of how closely the model aligns with human annotations. Additionally, AMBER (Wang et al., 2023), a fine-grained benchmark for generative tasks, provided key metrics such as CHAIR variants, object coverage, hallucination rates, and cognitive hallucination rates. This benchmark gives insight into the model’s generative performance and its ability to handle complex reasoning tasks without introducing hallucinations. Lastly, we further validated our model using LLaVA-Bench (Liu et al., 2024b), a benchmark covering systematic comprehension across various tasks such as conversation, detailed description, and answering complex questions. This comprehensive evaluation setup ensures a robust assessment of the model’s performance in both generative and interpretative tasks.

A.2 Baselines Details.

For a comprehensive evaluation, we compare our model with several state-of-the-art baselines across various categories. For general MLLMs, we evaluate against LLaVA1.5 (Liu et al., 2024a), Qwen-VL-Chat (Bai et al., 2023), LLaVA1.6, and MiniGemini (Li et al., 2024). These models are trained on large-scale datasets and show strong performance across multiple benchmarks. For models utilizing preference feedback, we include POVID (Zhou et al., 2024), RLHF-V (Yu et al., 2024a), Silkie (Sun et al., 2023), and HA-DPO (Zhao et al., 2023b), all of which employ reinforcement learning on preference data and achieve competitive results. In the feedback-independent category, we evaluate VCD (Leng et al., 2024), OPERA (Park et al., 2024), and EOS (Yue et al., 2024), which focus on decoding optimizations without using preference data. Finally, we include GPT-4V (Achiam et al., 2023), a proprietary black-box model, to benchmark our model against the strongest commercial system.

B Related Work

Preference Alignment for Trustworthiness.

Preference alignment is widely applied in LLMs and MLLMs to enhance their trustworthiness and reduce visual hallucinations (Stienon et al., 2020; Bai et al., 2022; Ouyang et al., 2022; Chen et al.,

2024c,b). MLLMs alignment approaches primarily lie in two categories: manual construction of preference pairs and automatic generation using MLLMs. RLHF-V (Yu et al., 2024a; Sun et al., 2023) uses human feedback to refine hallucinated captions, turning rejected responses into chosen ones. In contrast, Povid (Zhou et al., 2024; Pi et al., 2024) introduces diffusion noise to images, allowing MLLMs to automatically generate hallucinated content, which is used as rejected responses without human input. AMP (Zhang and Rong, 2024) improves stability by generating multiple candidate responses, while RLAIF-V (Yu et al., 2024b) refines DPO using high-quality responses from multiple MLLMs. However, these methods focus mainly on text preferences, often lacking balance between modalities, limiting their effectiveness in tasks that rely on detailed image information.